Engineered Science
DOI: http://dx.doi.org/10.30919/es1713

Metal-assisted Microwave Induction Method for Constructing Basal Plane and End-face Nanostructures of High-quality Graphene

Jie Zhang,[1, 2,*] Tong Wang[1, 2] and Min Gu[1, 2,*]

Abstract

Most commercial graphene is prepared by exfoliation, redox processes, chemical vapor deposition (CVD), *etc*. Although some methods have been featured for high-quality graphene or massive productivity, they require high-energy cost treatment or environmentally unfriendly chemicals, which may lead to defective structures or low yields. Here, we describe the use of metal-assisted microwave induction (MAMI) to generate high-energy density plasma to effectively remove the remaining functional groups of the carbon source material in seconds. The removal step is followed by the peeling off single-layer material to reorder basal plane and end surface, establishing a sequential crystal structure. To our knowledge, in this study, the world-record for the highest graphene Raman spectroscopy of 2D/G band intensity ratio (~12) via proposed method is achieved for microwave-irradiated carbon black (MICB). Meanwhile, a world-record low-intensity D/G band (0.0034) in Raman spectroscopy is revealed, suggesting that MICB contains ultralow defect concentrations, clearly proving the turbostratic structure in the microwave-irradiated carbon materials. The strong interlayer interaction in turbostratic graphene layers significantly strengthens intervalley resonance scattering, attributing to the mirror symmetry of the valence and conduction bands relative to the Fermi level near the Dirac point in the Brillouin zone, result in a notable increase of the 2D peak intensity. The almost perfect single Lorentzian line shape fitting of 2D peak indicates either only single layer graphene or turbostratic graphene where 2-dimensional structure generated while the defect density is calculated to be ~7.5×108 cm-2 according to D/G band ratio. The conductivity can increase when the functional groups are eliminated followed by decreased D peak. Consequently, highly reproducible and excellent quality materials synthesized from low-cost carbon source materials such as bamboo, coconut shell, rice shell, wood via MAMI can be used for universal preparations and applications of graphene. The electric energy consumed is estimated to be ~0.6 kilojoules per gram.

Keywords: Microwave; Graphene; Raman scattering; Supercapacitors.
Received: 25 March 2025; Revised: 11 July 2025; Accepted: 24 August 2025.
Article type: Research article.

1. Introduction

Microwave radiation methods have been widely applied in industrially scalable and facile fabrication approaches to produce high-quality and low-cost graphene.[1-3] However, owing to the limited exploitation of microwave energy, high-electronic-quality graphene has yet to be guaranteed. To our knowledge, among all graphene preparation methods, two techniques have achieved exceptionally high-quality graphene, where significantly higher-intensity 2D bands and lower-intensity D bands of Raman spectra far exceeding those of traditional spectra have been recorded; nevertheless, these methods have low specific surface areas with flash graphene synthesis and low yields with CVD method.[4,5] Other major graphene synthesis methods such as reduced graphene oxide,[1,6] mechanical exfoliation,[7] and epitaxial graphene on silicon carbide,[8] also secure good quality graphene for single layer structure with similar issues above, environment unfriendly, or high cost. Here, we incorporate auxiliary metals and carbon source materials in a microwave oven for a short endurance time (in seconds, as the main process of the MAMI method) to build up the extremely low defect concentration

[1] *School of Artificial Intelligence Science and Technology, University of Shanghai for Science and Technology, Shanghai, 200093, China*
[2] *Institute of Photonic Chips, University of Shanghai for Science and Technology, Shanghai, 200093, China*
**E-mail*: jiezhang@usst.edu.cn (J. Zhang); gumin@usst.edu.cn (M. Gu)

and high electronic quality of graphene, as revealed by the low-intensity D band and unusually high 2D band in the Raman spectra.[9] Traditionally, placing metal in a microwave field is strictly prohibited because sparks are released on the surface of the metal (even when guided by the manufacturers of most microwave instruments in the manual). Nevertheless, the unique and powerful energy resulting from such phenomena is not fully understood. We have developed a novel and low-cost method for preparing high-quality graphene via a metal-assisted microwave induction (MAMI) technique. Metals are introduced to generate a high-energy-density plasma with help of microwave field to obtain high reaction temperature in milliseconds, which the carbon source materials cannot achieve along in the microwave field. The X-ray diffraction (XRD) and high-resolution transmission electron microscopy (HR-TEM) results suggest a desirable crystal structure. The temperature variation curve for MICB during the MAMI process reveals an ultrahigh material cooling speed of more than 300,000 °C/s, while the temperature range is controlled effectively by adjusting the microwave reaction power and time with the assistance of accessional metals; high temperatures and material cooling speeds are critical for producing high-quality graphene.[4,10] X-ray photoelectron spectroscopy (XPS) revealed that oxygen functional groups (C–O, C=O, *etc*.) were removed from carbon black (CB) during the microwave radiation process. These findings demonstrate that MAMI is a simple and efficient technique essential for preparing large quantities of single-layer two-dimensional materials that do not introduce other chemicals.

2. Experimental section/methods

2.1 Materials

Carbon materials were obtained from Nanjing XF NANO Materials Tech Co., Ltd., China. Li_2SO_4 was purchased from Sigma Aldrich, China, and the membrane was obtained from NKK, Japan. Titanium foil was used as the current collector layer from Jiazhi Metal Co., Ltd, China. The sealing film was purchased from Tianjin Annuohe New Energy Tech Co., Ltd, China.

2.2 Fabrication

A household Panasonic microwave oven (1,000 W) is used for the microwave reaction. Different proportions of various carbon source materials or their precursors, such as carbon black, graphene oxide, and graphite, are mixed thoroughly with auxiliary metals (iron, cobalt, nickel, aluminum, titanium, tungsten, holmium, silver, *etc*.) in foil, powder, irregular blocks, lumps, coils, twisted wires or other forms and placed in a quartz container and then placed in a microwave oven. Here, the strongest microwave peak intensity location may occur because of the possibility of generating stationary waves in a particular chamber of the microwave oven. The combinations are placed in a microwave chamber and radiated repeatedly several times under different atmospheres (air, nitrogen, argon, vacuum, or others) at atmospheric or low pressures varying from 0.1 to 10^5 Pa. After the microwave reaction was repeated (10 s to 120 s), an electromagnet is used to separate the iron from the reaction materials. Li_2SO_4 is prepared to make the 1.0 M aqueous electrolyte. Finally, the carbon powders are encapsulated into supercapacitors to test their performance.

2.3 Characterization

The Raman spectra are measured via a HORIBA microscope, and a 532-nm laser is introduced. Raman spectra are measured using a 50× lens. SEM images are taken with a Zeiss Sigma 300. High-resolution transmission electron microscopy (HRTEM) images are acquired with a JEOL JEM-2100Plus instrument. BET measurements are conducted with an ASAP 2460 instrument. XRD is performed with a Rigaku Ultima IV instrument. XPS is performed with a Thermo Scientific K-Alpha. The sample temperature is measured via an ultrafast color comparison IR temperature sensor CIT-1MDF. The electrochemical characteristics are obtained on a Gamery Interface 1010E.

3. Results and discussion

In the MAMI process, carbon source materials or their precursors are mixed thoroughly with auxiliary metals and placed in a quartz container. The metals can be iron, cobalt, nickel, titanium, tungsten, holmium, silver, *etc*., in the form of powder, foil, lumps, wires or any irregular size. Then, the mixture is placed in a microwave chamber under different atmospheres (air, nitrogen, argon, vacuum, or others) at atmospheric or low pressure (~0.1 Pa) to release gas pressure during the reaction process (Fig. 1(a), Fig. S3, and Fig. S6) [see the "Fabrication" section in the Methods section]. Via the structural information provided by Raman spectroscopy, high-quality graphene can be distinguished over square-micrometer regions.[4,5,11,12] As shown in Fig. 1(b), a high 2D band intensity versus G band intensity (I_{2D}/I_G: ~12) was obtained via this technique, indicating turbostratic structure with high electronic quality.[11,13,14] This is the highest value reported to date for microwave treatment technologies.[15] Additionally, the D band can barely be detected, indicating extremely low defect concentrations, which suggests excellent-quality graphene where two Raman spectroscopy peaks TS_1 and TS_2 at 1,880 cm^{-1} and 2,030 cm^{-1} appear in MICB (Fig. S11). As shown in Fig. S1(c), the best I_D/I_G peak area ratio is less than 3.4×10^{-3}. The relevant defect density is calculated to be

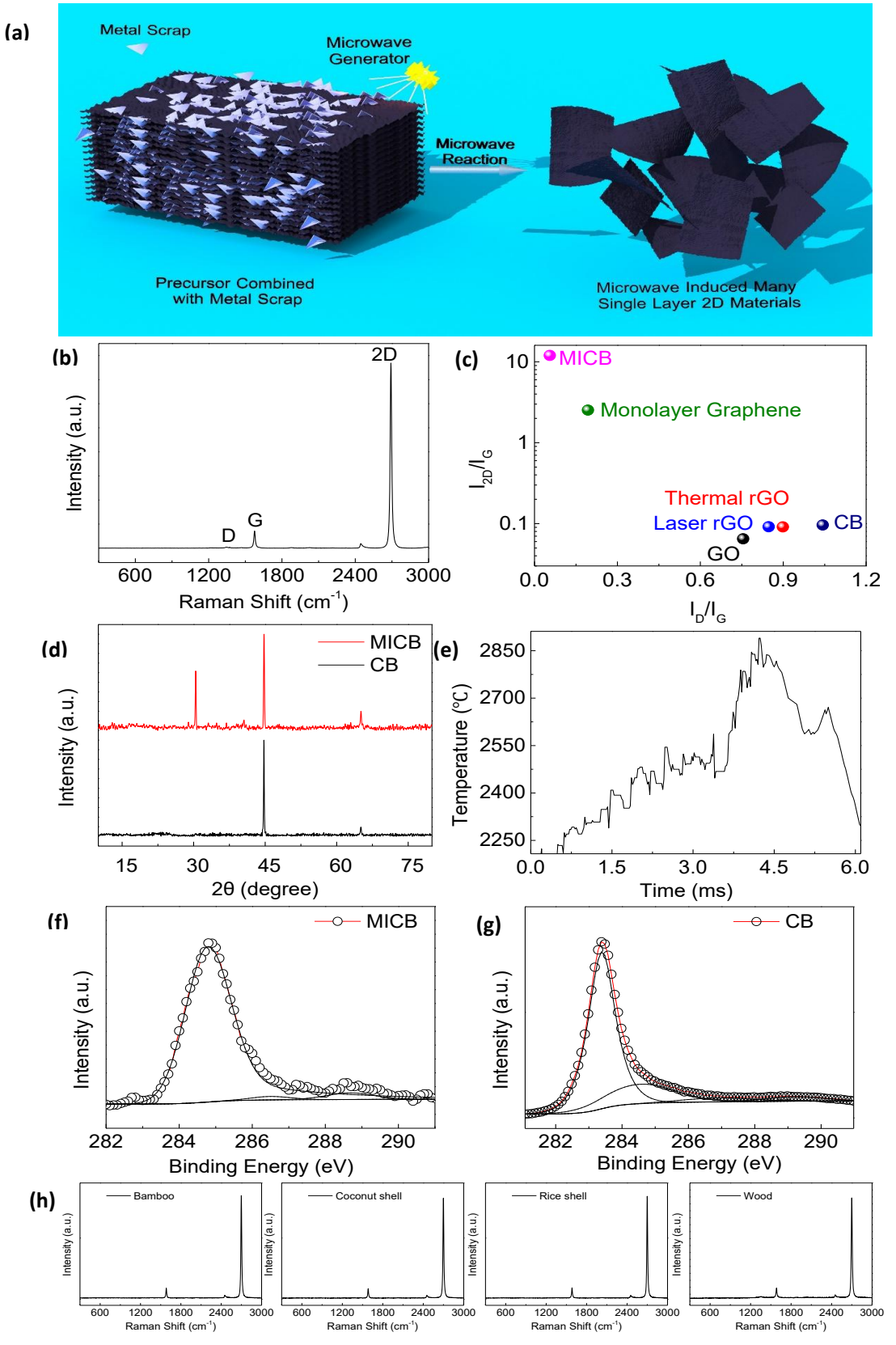

Fig. 1: MICB synthesis with the MAMI treatment. (a) MAMI method process illustration. (b) Best Raman spectra obtained from MICB materials. (c) Development tendency of the 2D band versus the D band along with normalized G band for different carbon materials. (d) XRD spectra images where auxiliary metal (iron) appeared in the samples. (e) Temperature record for the MICB during the MAMI method process. (f, g) XPS results for MICB and CB. (h) Best Raman spectra obtained from MAMI method proceeded bamboo, coconut shell, rice shell, and wood.

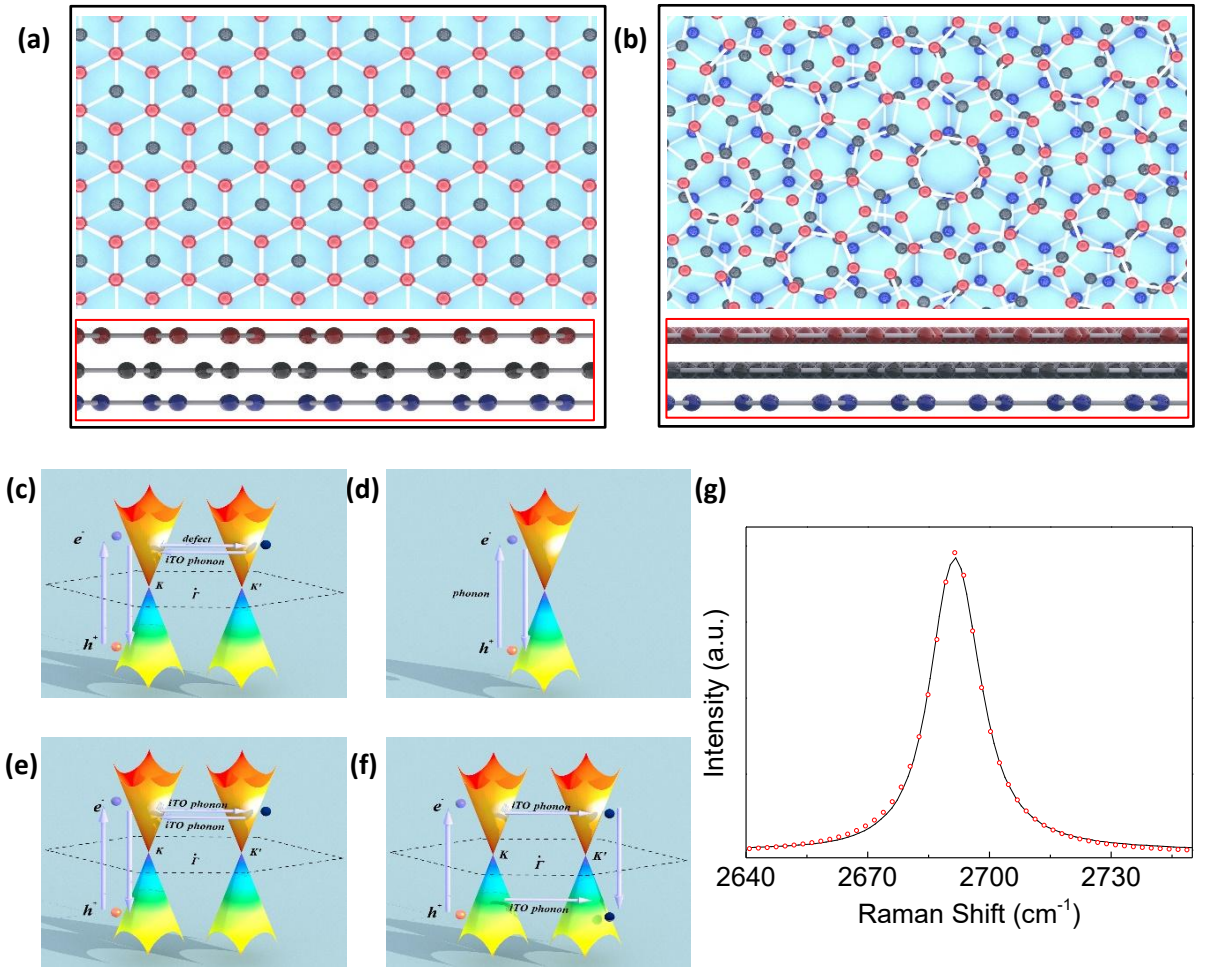

Fig. 2: Analysis of turbostratic structure graphene for novel Raman spectrum. (a-b) Top view of AB Bernal stacking graphene layers, inset cross-section view, and turbostratic structure graphene layers, inset cross-section view. (c-f) Origination of graphene's Raman Stokes spectrum for D peak; G peak; and 2D peak. (g) 2D peak of Raman for MICB shows almost a perfect Lorentzian line shape (red dots) with R^2 for the correlation 0.99864.

~7.5×10^8 cm^{-2} according to D/G band ratio.[5,16] The mean Raman spectra and Raman intensity mapping for the I_{2D}/I_G peak area ratio are shown in Fig. S1 and cover an area of ~672 μm^2 at 50× magnification. Even average Raman spectroscopy of I_{2D}/I_G peak area ratio for MICB suggests excellent quality compared with that of graphene produced by traditional technologies. During the microwave radiation process, a sample is heated to 2,890 °C/s in ~4.2 ms as a result of the interaction of the strong microwave power and plasma generated during the reaction process. Subsequently, the sample cooled to 2,300 °C/s in ~1.8 ms due to thermal transportation. Such ultrafast heating and cooling speeds are critical to the initiation of the crystal structure of high-quality graphene, which is derived from the interaction of auxiliary metals and the microwave field; otherwise, a low microwave power, an improper reaction time or absence of auxiliary metals reduces the I_{2D}/I_G ratio, leading to low-quality graphene (Fig. S8).[1,2,10,17]

As one of sp^2 carbons, the energy transportation mechanism and formation of this high quality graphene has been disclosed in previous theoretical study, where it is revealed that a suitable carbon material temperature (~3,000 K) helps repair local non-hexagonal rings and the holes of graphene via local atomic rearrangement owing to adatoms.[18] The turbostratic arrangement of MAMI-proceeded carbon materials allows multiple possibility for twisted. graphene layers at different angles, distinct from the conventional AB Bernal stacking (Fig. 2). At specific twist angle, the probability of intervalley double-resonance or even triple-resonance scattering increases due to the lower energy of interlayer electronic resonant states compared to AB Bernal stacking graphene layers.[19-21] Furthermore, variations in interlayer spacing within MAMI-synthesized carbon materials alter interlayer bonding energies, leading to active graphene layers with fluctuation. Phonon dispersion plots reveal six phonon branches (iLO, iTO, oTO, iLA, iTA and oTA) near the

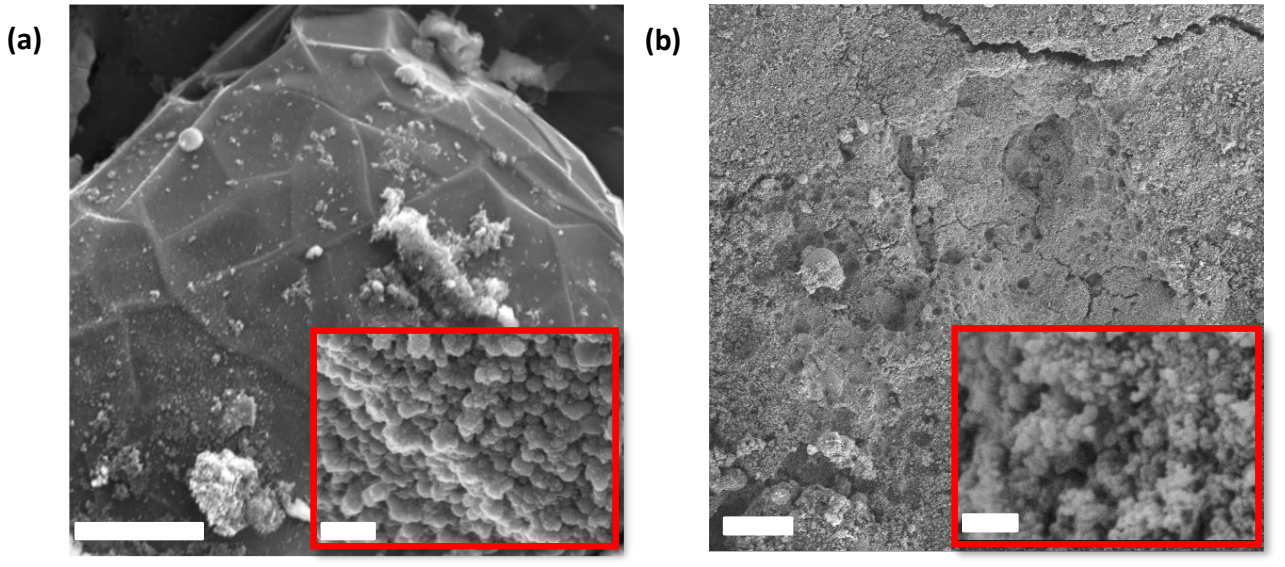

Fig. 3: SEM images show different morphologies before and after the MAMI process. (a) MICB and (b) original CB. The scale bar is 6 μm, and the scale bar in the inset images is 200 nm.

Γ and K points, for a single-layer graphene unit cell, which contains two carbon atoms, where three branches are optic (O), and the other three are acoustic (A).[21] In graphene's Raman Stokes spectrum, the D peak originates from second-order intervalley scattering involving one iTO phonon and one defect; the G peak is the only peak result from a normal first order Raman scattering where associated with the double-degenerate iTO and iLO phonons with E_{2g} symmetry resonance at the Brillouin zone center; the 2D peak arises from two iTO phonons participating in intervalley double-resonance scattering or triple-resonance scattering near the Dirac (K) point shown in Figs. 2(c-f). The strong interlayer interaction in turbostratic graphene layers significantly strengthens intervalley resonance scattering. This phenomenon is attributed to the mirror symmetry of the valence and conduction bands relative to the Fermi level near the K point in the Brillouin zone, while electronic defect states have been repaired, result in a notable increase in the intensity of the 2D peak.[19,22] Unlike AB Bernal stacking bilayer, trilayer and other multilayer graphene where the 2D peak splits into four, six and multiple Lorentzian peaks, due to altered electronic band structures near the Fermi level, MAMI-synthesized carbon materials exhibit a single Lorentzian profile shown in Fig. 2(g), This indicates the presence of a perfectly mirrored conical Dirac cone at the K point.[13,23-28] Moreover, the MAMI method offers a cost-effective and energy-efficient approach, consuming approximately ~0.6 kilojoules per gram. This is significantly more economical compared to traditional graphene synthesis techniques, such as CVD, chemical reduction, and mechanical exfoliation.

Moreover, the choices for types of auxiliary metals seem to exhibit partial differences due to their electric conductivity, magnetic conductivity, shape, melting point, chemical activity, robustness, stability (Fig. S2(b)), *etc*. Magnetic materials share comprehensive advantages, such as good electric and magnetic conductivity, high-temperature resistance, low chemical activity in the inner atmosphere, easy separation from MICB, low cost, and reusability after microwave reactions, and are barely consumed during MAMI treatment. Most conductive materials are capable of generating high-energy plasma in a microwave field with chemical activities that vary with different metal types and ambient gas types owing to the principles of electron excitation and transition induced by conductive material ions and gas ions at high temperatures.[29] For the same introduced metal, the surface charge density increases rapidly in a strong electric field, making it easy for the metal close to the carbon source materials to discharge to the surrounding gas or adjacent materials. Under the influence of the strong variational electromagnetic field on the surface of the conductor, the residual ions in the nearby gas undergo intense motion and collide violently with the surrounding molecules, leading to ionized molecules and many positive and negative ions continuously occurring. The reactions are well controlled inside the container, minimizing possible hazards caused to the reactor. The simulation in Fig. S9 proves that even carbon materials during the MAMI process can generate a strong electric field intensity of 2.13×10^7 V/m to initiate the production of high-quality graphene. The XRD patterns show that the amorphous carbon source materials are well radiated

by a strong microwave field into the highly ordered crystal structure of graphene, where the (002) peak appears. The slight drift of the (002) peak is due to the high compact pressure (greater than 12 MPa) applied during precursor preparation for good contact.[30] The well-treated MICB has a large specific surface area of 1,357.39 m²/g, as measured by Brunauer-Emmett-Teller (BET) area analysis (Fig. S5), which increased from 1,061.18 m²/g for CB. The XPS comparison between MICB and CB indicates that oxygen functional groups (C–O, C=O, *etc*.) are effectively removed from CB during the microwave radiation process. The full width at half maximum of the MICB XPS peak is slightly larger than that of the CB peak, indicating that residual amorphous carbon has been radiated to a minimum scale.[31] By introducing such efficient method, carbon-source materials obtained from MAMI proceeded bamboo, coconut shell, rice shell, and wood also show excellent quality revealed from Raman spectra.

Unlike previous studies of graphene morphologies, MICB shows unusual highly ordered structures of hundreds of square micrometers, as revealed by both scanning electron microscopy (SEM) and optical images (Fig. 3(a), Figs. S1(d-f)) corresponding to those samples of Raman measurements. Multiple glossy irregular disjunctive areas of MICB contribute to high-quality graphene at the sub-micrometer scale. High-magnification SEM images revealed that after MAMI treatment, randomly arranged CB powders radiated into ordered, low-roughness porous structures with many sequential nanosized interstitial sites; these structures can facilitate charge carrier transport and ohmic contact when MICB is applied in energy storage devices, such as supercapacitors and batteries.[32-35] Although previous studies created ultrasmooth and flat graphene for flexible devices,[36,37] limited charge carrier channels were generated. Most high-quality MICB are found in these smooth disjunctive regions, suggesting an essential morphological structure for microwave-irradiated carbon source materials, where these nanostructures (shown in Fig. S4) correspond to a large specific surface area. A further survey of the morphologies of MICB and CB revealed that the typical diameter sizes of their basic nanoparticles are 31.25 nm and 26.50 nm, respectively. Despite the larger volume of ordered nanoparticles in MICB than in untreated CB, the specific surface area of MICB increased by 27.91% after the microwave irradiation process. This is because carbon materials undergo rapid expansion and

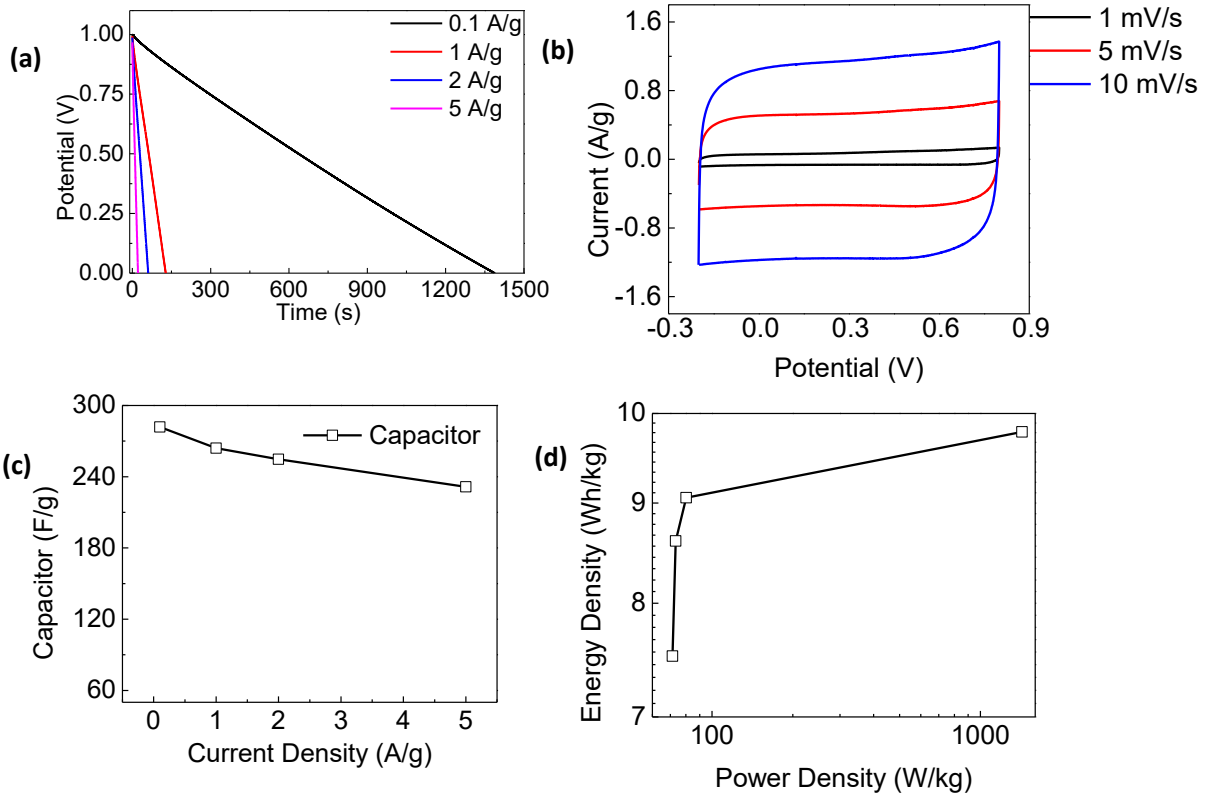

Fig. 4: Electrochemical characterization of a supercapacitor based on MICB materials in 3.0 M Li_2SO_4. (a) Charging/discharging curves with various current densities. (b) CV curves at 1 mV/s, 5 mV/s, and 10 mV/s. (c) Gravimetric capacitances with various charging/discharging current densities. (d) Ragone plots of the MICB-based supercapacitor.

exfoliation processes with considerable temperature variation.[38-40] By increasing the sample temperature to more than 3,000 K and subsequently decreasing the temperature to less than 2,500 K in milliseconds, both the sample volume and specific surface area increase. In addition, the high-energy plasma generated in the microwave field guarantees high-quality graphene, leading to excellent MICB assisted by the applied metal.

Using the best-practice MAMI methods to determine whether an electrode material's performance is suitable for supercapacitors, we constructed and measured the performance of two-electrode symmetrical supercapacitor cells on the basis of the MICB (shown in Fig. S7) and Li_2SO_4 electrolytes.[41,42] The cyclic voltammetry tests reveal rectangular curves over a typical range of voltage scan rates. The galvanostatic charge/discharge curves at different current densities are shown in Fig. 4(a). The corresponding capacitance is 281.86 F/g. The voltage drop at the initiation of discharge is 0.02 mV (for a current density of 0.1 A/g), suggesting a very low equivalent series resistance (ESR) in the test cell.[43] The voltage drop at the beginning of the discharge curves is used to estimate the internal resistance. An ESR of 0.10 mohms is obtained from the MICB in the Li_2SO_4 electrolyte. The values for energy and power density are estimated on the basis of MICB supercapacitor measurements. Using a specific capacitance value of 281.86 F/g (from the discharge curve with a constant current of 0.1 A/g) and a working voltage window of 1.0 V, the energy density is 9.79 Wh/kg. At the same current density, the power density is 1428.41 W/kg, as estimated from the voltage drop and ESR obtained from the discharge curve.[44] We believe that these carbon materials might perform even better with other diameter ions.[45-47]

4. Conclusion

In summary, we exhibit an efficient and cost-effective methods for producing high-quality MAMI graphene where one step is required to realize such synthesis. By introducing this efficient method, low-cost carbon-source materials obtained from MAMI proceeded bamboo, coconut shell, rice shell, and wood also show excellent quality revealed from Raman spectra. The unique performance of aqueous electrolytes makes it possible to engineer supercapacitor electrodes based on this form of carbon to target a wide range of applications, such as high-energy, high-power, high-efficiency, or low-cost supercapacitors. Unlike other carbon materials, no special substrates or transfer procedures are required for synthesis. The novel phenomena of MAMI prepared carbon material's Raman spectrum are discussed that the strong interlayer interaction in turbostratic graphene layers significantly strengthens intervalley resonance scattering, attributing to the mirror symmetry of the valence and conduction bands relative to the Fermi level near the Dirac point in the Brillouin zone, result in a notable increase of the 2D peak intensity and ultra-low D peak. For supercapacitors, batteries or other energy storage devices, this material can be treated the same as current commercial electrodes. As previously stated, the processes used to synthesize this carbon material are readily scalable to industrial levels (Figs. S10 and S12). By introducing this type of simple and low-cost activation process, scaled MICB production for advanced energy/power electrical energy storage devices may be realized in a short period.

Acknowledgements

The authors acknowledge the financial support from the Natural Science Foundation of China and Xi Chen, Min Gu for helpful discussion. This work made use of the facilities at the University of Shanghai for Science and Technology for Electron Microscopy. The authors gratefully acknowledge support from the Shanghai Pujiang Program (Grant No. 23PJ1409700), the Shanghai Science and Technology Program (Grant No. 21ZR1445500) and the National Natural Science Foundation of China (Grant Nos. 11974247 and 62175154).

Conflict of Interest

There is no conflict of interest.

Supporting Information

Applicable.

CRediT Statement

Jie Zhang: Conceiving & designing, Performing fabrication, Optimization, Characterization, Writing, Review & Editing, Funding acquisition, Original draft, Methodology, Investigation, Formal analysis, Data curation (lead). **Tong Wang:** Performing SEM measurements. **Min Gu**: Supervision (lead).

References

[1] D. Voiry, J. Yang, J. Kupferberg, R. Fullon, C. Lee, H. Y. Jeong, H. S. Shin, M. Chhowalla, High-quality graphene *via* microwave reduction of solution-exfoliated graphene oxide, *Science*, 2016, **353**, 1413-1416, doi: 10.1126/science.aah3398.

[2] Y. Sun, L. Yang, K. Xia, H. Liu, D. Han, Y. Zhang, J. Zhang, "Snowing" graphene using microwave ovens, *Advanced Materials*, 2018, **30**, 1803189, doi: 10.1002/adma.201803189.

[3] H. M. A. Hassan, V. Abdelsayed, A. EI Rahman S. Khder, K. M. AbouZeid, J. Terner, M. S. El-Shall, S. I. Al-Resayes, A. A.

El-Azhary, Microwave synthesis of graphene sheets supporting metal nanocrystals in aqueous and organic media, *Journal of Materials Chemistry*, 2009, **19**, 3832-3837, doi: 10.1039/B906253J.

[4] D. X. Luong, K. V. Bets, W. Ali Algozeeb, M. G. Stanford, C. Kittrell, W. Chen, R. V. Salvatierra, M. Ren, E. A. McHugh, P. A. Advincula, Z. Wang, M. Bhatt, H. Guo, V. Mancevski, R. Shahsavari, B. I. Yakobson, J. M. Tour, Gram-scale bottom-up flash graphene synthesis, *Nature*, 2020, **577**, 647-651, doi: 10.1038/s41586-020-1938-0.

[5] J. Amontree, X. Yan, C. S. DiMarco, P. L. Levesque, T. Adel, J. Pack, M. Holbrook, C. Cupo, Z. Wang, D. Sun, A. J. Biacchi, C. E. Wilson-Stokes, K. Watanabe, T. Taniguchi, C. R. Dean, A. R. Hight Walker, K. Barmak, R. Martel, J. Hone, Reproducible graphene synthesis by oxygen-free chemical vapour deposition, *Nature*, 2024, **630**, 636-642, doi: 10.1038/s41586-024-07454-5.

[6] T. Kuanyshbekov, N. Guseinov, B. Kurbanova, R. Nemkaeva, K. Akatan, Z. Tolepov, M. Tulegenova, M. Aitzhanov, E. Zhasasynov, S. Thomas, Local natural graphite as a promising raw material for the production of thermally reduced graphene-like films, *ES Materials & Manufacturing*, 2023, **23**, 1000, doi: 10.30919/esmm1000.

[7] K. S. Novoselov, A. K. Geim, S. V. Morozov, D. Jiang, Y. Zhang, S. V. Dubonos, I. V. Grigorieva, A. A. Firsov, Electric field effect in atomically thin carbon films, *Science*, 2004, **306**, 666-669, doi: 10.1126/science.1102896.

[8] G. Yazdi, T. Iakimov, R. Yakimova, Epitaxial graphene on SiC: a review of growth and characterization, *Crystals*, 2016, **6**, 53, doi: 10.3390/cryst6050053.

[9] N. Sharma, S. Tomar, M. Shkir, R. Kant Choubey, A. Singh, Study of optical and electrical properties of graphene oxide, *Materials Today: Proceedings*, 2021, **36**, 730-735, doi: 10.1016/j.matpr.2020.04.861.

[10] S. Zhu, F. Zhang, H. G. Lu, J. Sheng, L. Wang, S. D. Li, G. Han, Y. Li, Flash nitrogen-doped graphene for high-rate supercapacitors, *ACS Materials Letters*, 2022, **4**, 1863-1871, doi: 10.1021/acsmaterialslett.2c00616.

[11] A. C. Ferrari, J. C. Meyer, V. Scardaci, C. Casiraghi, M. Lazzeri, F. Mauri, S. Piscanec, D. Jiang, K. S. Novoselov, S. Roth, A. K. Geim, Raman spectrum of graphene and graphene layers, *Physical Review Letters*, 2006, **97**, 187401, doi: 10.1103/physrevlett.97.187401.

[12] Z. H. Ni, T. Yu, Z. Q. Luo, Y. Y. Wang, L. Liu, C. P. Wong, J. Miao, W. Huang, Z. X. Shen, Probing charged impurities in suspended graphene using Raman spectroscopy, *ACS Nano*, 2009, **3**, 569-574, doi: 10.1021/nn900130g.

[13] J. A. Garlow, L. K. Barrett, L. Wu, K. Kisslinger, Y. Zhu, J. F. Pulecio, Large-area growth of turbostratic graphene on Ni(111) *via* physical vapor deposition, *Scientific Reports*, 2016, **6**, 19804, doi: 10.1038/srep19804.

[14] A. Niilisk, J. Kozlova, H. Alles, J. Aarik, V. Sammelselg, Raman characterization of stacking in multi-layer graphene grown on Ni, *Carbon*, 2016, **98**, 658-665, doi: 10.1016/j.carbon.2015.11.050.

[15] R. Johnson, M. A. Zafar, S. Thomas, M. V. Jacob, A critical review on vacuum and atmospheric microwave plasma-based graphene synthesis, *FlatChem*, 2025, **50**, 100812, doi: 10.1016/j.flatc.2025.100812.

[16] L. G. Cançado, A. Jorio, E. H. Martins Ferreira, F. Stavale, C. A. Achete, R. B. Capaz, M. O. Moutinho, A. Lombardo, T. S. Kulmala, A. C. Ferrari, Quantifying defects in graphene *via* Raman spectroscopy at different excitation energies, *Nano Letters*, 2011, **11**, 3190-3196, doi: 10.1021/nl201432g.

[17] C. Casiraghi, A. Hartschuh, H. Qian, S. Piscanec, C. Georgi, A. Fasoli, K. S. Novoselov, D. M. Basko, A. C. Ferrari, Raman spectroscopy of graphene edges, *Nano Letters*, 2009, **9**, 1433-1441, doi: 10.1021/nl8032697.

[18] Y. Huang, Q. Gong, Q. Zhang, Y. Shao, J. Wang, Y. Jiang, M. Zhao, D. Zhuang, J. Liang, Fabrication and molecular dynamics analyses of highly thermal conductive reduced graphene oxide films at ultra-high temperatures, *Nanoscale*, 2017, **9**, 2340-2347, doi: 10.1039/C6NR06653D.

[19] Z. Dai, Z. Gao, S. S. Pershoguba, N. Tiwale, A. Subramanian, Q. Zhang, C. Eads, S. A. Tenney, R. M. Osgood, C. Y. Nam, J. Zang, A. T. Charlie Johnson, J. T. Sadowski, Quantum-well bound states in graphene heterostructure interfaces, *Physical Review Letters*, 2021, **127**, 086805, doi: 10.1103/PhysRevLett.127.086805.

[20] I. Kupčić, Triple-resonant two-phonon Raman scattering in graphene, *Journal of Raman Spectroscopy*, 2012, **43**, 1-5, doi: 10.1002/jrs.3003.

[21] L. M. Malard, M. A. Pimenta, G. Dresselhaus, M. S. Dresselhaus, Raman spectroscopy in graphene, *Physics Reports*, 2009, **473**, 51-87, doi: 10.1016/j.physrep.2009.02.003.

[22] S. J. Ahn, P. Moon, T. H. Kim, H. W. Kim, H. C. Shin, E. H. Kim, H. W. Cha, S. J. Kahng, P. Kim, M. Koshino, Y. W. Son, C. W. Yang, J. R. Ahn, Dirac electrons in a dodecagonal graphene quasicrystal, *Science*, 2018, **361**, 782-786, doi: 10.1126/science.aar8412.

[23] D. Graf, F. Molitor, K. Ensslin, C. Stampfer, A. Jungen, C. Hierold, L. Wirtz, Spatially resolved Raman spectroscopy of single- and few-layer graphene, *Nano Letters*, 2007, **7**, 238-242, doi: 10.1021/nl061702a.

[24] Z. Ni, Y. Wang, T. Yu, Z. Shen, Raman spectroscopy and imaging of graphene, *Nano Research*, 2008, **1**, 273-291, doi: 10.1007/s12274-008-8036-1.

[25] M. S. Dresselhaus, A. Jorio, M. Hofmann, G. Dresselhaus, R. Saito, Perspectives on carbon nanotubes and graphene Raman

spectroscopy, *Nano Letters*, 2010, **10**, 751-758, doi: 10.1021/nl904286r.
[26] F. Schedin, E. Lidorikis, A. Lombardo, V. G. Kravets, A. K. Geim, A. N. Grigorenko, K. S. Novoselov, A. C. Ferrari, Surface-enhanced Raman spectroscopy of graphene, *ACS Nano*, 2010, **4**, 5617-5626, doi: 10.1021/nn1010842.
[27] R. Saito, M. Hofmann, G. Dresselhaus, A. Jorio, M. S. Dresselhaus, Raman spectroscopy of graphene and carbon nanotubes, *Advances in Physics*, 2011, **60**, 413-550, doi: 10.1080/00018732.2011.582251.
[28] A. Eckmann, A. Felten, A. Mishchenko, L. Britnell, R. Krupke, K. S. Novoselov, C. Casiraghi, Probing the nature of defects in graphene by Raman spectroscopy, *Nano Letters*, 2012, **12**, 3925-3930, doi: 10.1021/nl300901a.
[29] P. Mehta, P. Barboun, D. B. Go, J. C. Hicks, W. F. Schneider, Catalysis enabled by plasma activation of strong chemical bonds: a review, *ACS Energy Letters*, 2019, **4**, 1115-1133, doi: 10.1021/acsenergylett.9b00263.
[30] Z. Q. Li, C. J. Lu, Z. P. Xia, Y. Zhou, Z. Luo, X-ray diffraction patterns of graphite and turbostratic carbon, *Carbon*, 2007, **45**, 1686-1695, doi: 10.1016/j.carbon.2007.03.038.
[31] S. Kim, S. Zhou, Y. Hu, M. Acik, Y. J. Chabal, C. Berger, W. de Heer, A. Bongiorno, E. Riedo, Room-temperature metastability of multilayer graphene oxide films, *Nature Materials*, 2012, **11**, 544-549, doi: 10.1038/nmat3316.
[32] K. S. Novoselov, V. I. Fal'ko, L. Colombo, P. R. Gellert, M. G. Schwab, K. Kim, A roadmap for graphene, *Nature*, 2012, **490**, 192-200, doi: 10.1038/nature11458.
[33] B. Kang, G. Ceder, Battery materials for ultrafast charging and discharging, *Nature*, 2009, **458**, 190-193, doi: 10.1038/nature07853.
[34] S. Wu, R. Ge, M. Lu, R. Xu, Z. Zhang, Graphene-based nano-materials for lithium–sulfur battery and sodium-ion battery, *Nano Energy*, 2015, **15**, 379-405, doi: 10.1016/j.nanoen.2015.04.032.
[35] H. Chen, H. Xu, S. Wang, T. Huang, J. Xi, S. Cai, F. Guo, Z. Xu, W. Gao, C. Gao, Ultrafast all-climate aluminum-graphene battery with quarter-million cycle life, *Science Advances*, 2017, **3**, eaao7233, doi: 10.1126/sciadv.aao7233.
[36] C. H. Lui, L. Liu, K. F. Mak, G. W. Flynn, T. F. Heinz, Ultraflat graphene. *Nature,* 2009, **462**, 339-341, doi: 10.1038/nature08569.
[37] X. Dai, J. Wu, Z. Qian, H. Wang, J. Jian, Y. Cao, M. H. Rummeli, Q. Yi, H. Liu, G. Zou, Ultra-smooth glassy graphene thin films for flexible transparent circuits, *Science Advances*, 2016, **2**, e1601574, doi: 10.1126/sciadv.1601574.
[38] A. Karaipekli, A. Sarı, K. Kaygusuz, Thermal conductivity improvement of stearic acid using expanded graphite and carbon fiber for energy storage applications, *Renewable Energy*, 2007, **32**, 2201-2210, doi: 10.1016/j.renene.2006.11.011.
[39] W. Wang, X. Yang, Y. Fang, J. Ding, J. Yan, Preparation and thermal properties of polyethylene glycol/expanded graphite blends for energy storage, *Applied Energy*, 2009, **86**, 1479-1483, doi: 10.1016/j.apenergy.2008.12.004.
[40] B. Wei, L. Zhang, S. Yang, Polymer composites with expanded graphite network with superior thermal conductivity and electromagnetic interference shielding performance, *Chemical Engineering Journal*, 2021, **404**, 126437, doi: 10.1016/j.cej.2020.126437.
[41] Q. Gao, L. Demarconnay, E. Raymundo-Piñero, F. Béguin, Exploring the large voltage range of carbon/carbon supercapacitors in aqueous lithium sulfate electrolyte, *Energy & Environmental Science*, 2012, **5**, 9611-9617, doi: 10.1039/C2EE22284A.
[42] Q. Gao, Optimizing carbon/carbon supercapacitors in aqueous alkali sulfates electrolytes, *Journal of Energy Chemistry*, 2019, **38**, 219-224, doi: 10.1016/j.jechem.2019.03.037.
[43] P. B. Dahivade, S. G. Randive, B. Y. Fugare, V. S. Sathe, A. V. Thakur, B. J. Lokhande, Nano-crystalline cadmium oxide thin films for supercapacitor application: effect of solution concentrations, *ES Energy & Environment*, 2024, **23,** 1105, doi: 10.30919/esee1105.
[44] K. Zhao, Z. Shi, Q. Li, Q. Li, F. Gao, Z. Yan, Performance of activated carbon from salvia miltiorrhiza roots as the electrode material for supercapacitors, *BioResources*, 2018, **13**, 4364-4377, doi: 10.15376/biores.13.2.4364-4377.
[45] M. F. El-Kady, V. Strong, S. Dubin, R. B. Kaner, Laser scribing of high-performance and flexible graphene-based electrochemical capacitors, *Science*, 2012, **335**, 1326-1330, doi: 10.1126/science.1216744.
[46] X. Yang, C. Cheng, Y. Wang, L. Qiu, D. Li, Liquid-mediated dense integration of graphene materials for compact capacitive energy storage, *Science*, 2013, **341**, 534-537, doi: 10.1126/science.1239089.
[47] P. Simon, Y. Gogotsi, Materials for electrochemical capacitors, *Nature Materials*, 2008, **7**, 845-854, doi: 10.1038/nmat2297.